Chaperone-mediated autophagy is an overlooked pathway for mutant α1-antitrypsin Z degradation

Jiayu Lin[1,2], Haorui Lu[2], Xinyue Wei[2,3], Yan Dai[1,2], Rihan Wu[4], Hao Yang[4]*, Lang Rao[1,2]*

1College of Biotechnology, Tianjin University of Science & Technology, Tianjin, 300457, China.

2National Technology Innovation Center of Synthetic Biology, Key Laboratory of Engineering Biology for Low–Carbon Manufacturing, Tianjin Institute of Industrial Biotechnology, Chinese Academy of Sciences, Tianjin 300308, China

3College of Life Science, Hebei Normal University, Shijiazhuang 050024, China

4Department of Radiation Oncology, Peking University Cancer Hospital (Inner Mongolia Campus) & Affiliated Cancer Hospital of Inner Mongolia Medical University, Huhhot, Inner Mongolia Autonomous Region, 010020, China.

* Address correspondence: yanghao0135@immu.edu.cn; raolang@tib.cas.cn

Abstract

Chaperone-mediated autophagy (CMA) is a specific form of autophagy that selectively targets proteins containing a KFERQ-like motif and relies on the chaperone protein HSC70 for substrate recognition. In α1-antitrypsin deficiency (AATD), a disease characterized by the hepatic build-up of α1-Antitrypsin Z mutant (ATZ), CMA's role had been unclear. This work demonstrates the critical role that CMA plays in preventing ATZ accumulation; suppressing CMA worsens ATZ accumulation, whilst activating it through chemical stimulation or LAMP2A overexpression promotes ATZ breakdown. Specifically, ATZ's 121QELLR125 motif is critical for HSC70 recognition and LAMP2A's charged C-terminal cytoplasmic tail is vital for substrate binding, facilitating CMA-mediated degradation of ATZ. This selective activation of CMA operates independently from other autophagy pathways and alleviate ATZ aggregates caused cellular stress. These findings highlight CMA's critical function in cellular protein quality control of ATZ and place it as a novel target for AATD treatment approaches.

Keywords

Chaperone-mediated autophagy, alpha-1 antitrypsin, protein degradation, LAMP2A, HSC70

Introduction

The autophagy-lysosome pathway is a major protein aggregate clearance mechanism that is conserved in all eukaryotic cells. This system can be classified into three main types based on their distinctive digestion processes: macroautophagy, microautophagy, and chaperone-mediated autophagy (CMA)[1]. Macroautophagy (referred to as autophagy) and microautophagy non-selectively engulf various substrates, whereas CMA specifically targets proteins containing the CMA-targeting KFERQ motif [2,3]. In CMA pathway, the heat shock cognate protein of 70 kDa (HSC70, also known as HSPA8) recognizes the KFERQ motif of substrate to form a substrate–chaperone complex [4], the complex was then delivered to lysosome surface to interact with the CMA specific receptor lysosome-associated membrane protein type 2A (LAMP2A). The LAMP2A in charge of delivering substrates directly to the lysosomal lumen for degradation [4,5]. Increasing evidence suggests that CMA plays a crucial role in various of physiological processes; CMA malfunction has been linked to a variety of diseases including neurodegenerative illnesses, metabolic disorders, lysosomal storage disorders and cancer [3] .

Alpha one antitrypsin (A1AT) is a serum protease inhibitor primarily synthesized in the liver and serves as a pulmonary neutrophil elastase neutralizer to protect the lung from self-elastolytic digestion. Thus, it plays a critical role in maintaining proper pulmonary proteolytic-inhibitor balance[6,7]. A1AT is a highly polymorphic protein, over 120 mutations in the *SERPINA1* gene have been identified and most mutation caused disease pathogenesis manifests as pulmonary emphysema because the loss of function as elastase neutralizer. These mutated A1AT caused manifestation is called alpha one antitrypsin deficiency (AATD). One genetic mutation result for a mutant protein ATZ with a E342K substitution exert the most sever phenotype. ATZ has misfolded conformation and prone to aggregate into insoluble polymers and The abnormal ATZ polymerization could result in liver cirrhosis [7,8]. Lung diseases resulting from AATD are treated with intravenous infusions of A1AT from donated human plasma , but this therapy does not mitigate liver damage caused by hepatic ATZ aggregates [9].

It has been established that, the ubiquitin–proteasome and autophagy–lysosomal pathways represent the two major routes for ATZ's bio-digestion [10,11]. Enhancing autophagy using

70 chemical compounds have all been shown to prohibit A1AT protein accumulation and
71 alleviating cell injury[12]. To date, there have been no studies exploring the role of CMA in the
72 regulation of ATZ catabolism. Theoretically, proteins with KFERQ motif could be recognized
73 by HSC70 and delivered for CMA degradation. Searching the sequence of ATZ, there is a
74 typical pentapeptide motifs within the ATZ sequence and those amino acids are exposed on the
75 surface of the protein molecular. This observation leads us to speculate that ATZ could be
76 targeted for CMA, and manipulating CMA might offer a solution for ATZ digestion, preventing
77 substantial polymerization.
78
79 **Material and methods:**

80 **Cell culture and plasmids transfection**

81 HEK 293 and HepG2 cells were obtained from the National Collection of Authenticated
82 Cell Cultures in Shanghai, China. The HeLa *ATG16L1-/-* and HeLa *BECLIN1-/-* cell lines were
83 provided by Dr. Yue Xu at Shanghai Jiao Tong University, China. All cells were cultured in
84 Dulbecco's Modified Eagle Medium (DMEM，FI101-01, TransGen Biotech) supplemented
85 with 10% fetal bovine serum (FBS，FI101-04, TransGen Biotech), 50 IU penicillin, and 50
86 μg/ml streptomycin under conditions of 37° C with a CO_2 concentration of 5%. Following the
87 manufacturer's instructions for transfection reagents (Lip8000, Beyotime), cells at a confluence
88 level of approximately 70% to 80% underwent plasmid transfection. Cells were then harvested
89 for further analysis after 48 to 72 hours post-transfection.

90 **Antibodies and Chemicals**

91 A1AT(8H10L18，ThermoFisher), LC3(AL221, Beyotime), Flag(AE005, AE169,
92 ABclonal), ATG16L1(AE3637, ABclonal), BECLIN1(A21191, ABclonal), β-Actin(AC026,
93 ABclonal), LAMP2A(AF1036, Beyotime), HRP Goat Anti-Rabbit IgG (H+L) (AS014,
94 ABclonal), HRP Goat Anti-Rabbit IgG (H+L)(AS003, ABclonal), ABflo® 594-conjugated
95 Goat Anti-Mouse IgG (H+L) (AS054, ABclonal), ABflo® 488-conjugated Goat Anti-Rabbit
96 IgG (H+L) (AS053, ABclonal) Cycloheximide(01810, Sigma), DMSO(D8371, Solarbo),
97 puromycin(P8230, Solarbo), streptomycin(P1400, Solarbo), AR7(HY-101106,

98 MedChemExpress), QX77(HY-112483, MedChemExpress), MG-132(HY-13259,
99 MedChemExpress), Chloroquine(HY-17589A, MedChemExpress).
100

101 **Molecular cloning and ShRNA knockdown**

102 *LAMP2A* and *HSC70* were cloned into pCDH-CMV (72265, Addgene) by PCR amplifying
103 the ORFs from cDNA templates of HSC70 (19514, Addgene) and LAMP2A (86146, Addgene),
104 followed by digestion with BamHI and EcoRI restriction enzymes. The molecular cloning was
105 performed using T4 DNA ligase and the resulting constructs were transformed into DH5α E.
106 coli cells. Plasmid purification and extraction steps were carried out using the Endo Free Mini
107 Plasmid Kit II (DP118, TIANGEN). ShRNA sequences are detailed in supplementary Figure 1,
108 and the corresponding shRNA plasmids were transfected into cells using Lip8000 transfection
109 reagent (C0533FT, Beyotime), following the manufacturer's protocol.

110 **Cloning of lentiviral expression constructs**

111 To develop GFP-ATZ and LAMP2A-expressing HEK 293 cells in a stable manner within
112 the pCDH-CMV vector using lentivirus, the *LAMP2A* and *ATZ* genes were amplified by PCR,
113 specifically targeting the ORFs from the cDNA templates of LAMP2A or SERPINA1. The
114 resulting cDNA insert of pCDH-CMV was then sub-cloned into the lentiviral backbone plasmid
115 pCHD-CMV-IRES-pur, thus constructing the pCDH-CMV-GFP-ATZ or pCDH-CMV-
116 LAMP2A plasmids. To generate lentiviral particles expressing the pCDH-CMV-GFP-ATZ or
117 pCDH-CMV-LAMP2A plasmids, the corresponding constructs were co-transfected with the
118 VSV-G and PVSV-2 helper plasmids into HEK 293 cells. The transfected cells were cultured
119 for 4 days to ensure sufficient expression time. Subsequently, the culture medium containing
120 viral particles was collected, filtered to remove debris, and used to infect HEK 293 cells,
121 inducing efficient expression of the target proteins within the host cells.

122 **Discovery and Mutations of the CMA Recognition Motif "KFERQ-like Pentapeptide"**

123 To demonstrate the involvement of CMA recognition motif, the complete amino acid

124 sequence of the *SERPINA1* gene was obtained by accessing the UniProt database (P01009). A
125 search was performed using the web server "KFERQ finder V0.8"
126 （https://rshine.einsteinmed.edu/）to identify pentapeptide sequences associated with the
127 CMA recognition motif. Within the amino acid sequence of *SERPINA1* (A1AT), a canonical
128 pentapeptide fragment, QELLR, was found at positions 121-125. To modify the physical
129 properties of amino acids within the targeting motif, as described by Orenstein and Cuervo [13],
130 we introduced mutations into the CMA recognition motif (5'-CAGGAACTCCTCCGT-3')
131 resulting in 5'-GCGGCACTCCTCCGT-3'. The mutated motif was then sub-cloned into a
132 pCDH-CMV plasmid.

133 **Fractionation of Cytoplasmic Soluble Proteins and Aggregates**

134 The cells were lysed using RIPA lysis buffer. After centrifugation at 13,000g for 10
135 minutes at 4°C, the supernatant was collected as the cytoplasmic soluble fraction, and the pellet
136 was resuspended in lysis buffer containing an additional 2% SDS. The resuspended pellet was
137 further homogenized by puncturing with a 28-gauge needle ten times.

138 **Immunoblotting**

139 Cell lysates were prepared in RIPA buffer to extract total protein. The obtained lysates
140 were then subjected to centrifugation at 17,000g for 20 minutes at 4°C to separate the soluble
141 lysates from the insoluble microspheres. Protein concentrations were determined using the
142 Bicinchoninic acid method, as directed by the manufacturer's instructions using the Pierce BCA
143 protein assay kit (23235, Thermo). Equal amounts of protein were transferred to a
144 polyvinylidene fluoride (PVDF) membrane through sodium dodecyl sulfate polyacrylamide gel
145 electrophoresis (SDS-PAGE). The primary antibody was added and incubated overnight at 4°C,
146 followed by incubation with the secondary antibody at room temperature for 45 minutes. Blot
147 was performed using a chemiluminescence kit (BeyoECL Plus P0018S, Beyotime) and visual
148 detection was performed using a western blotting detection system (Tienong 5200, China). The
149 gray values of protein bands in each group were subsequently quantified using ImageJ software,
150 and the ratio of target bands to β-actin bands was utilized as the measure of protein expression

151 level. The experiment was repeated three times with distinct protein samples.

152 **Immunoprecipitation**

153 To obtain the whole cell extract, the cells were treated with lysis buffer containing protease
154 inhibitor, and the resulting supernatant was collected. Magnetic beads (AC047, AE097,
155 ABclonal) were pre-treated with antibody binding and subsequently mixed thoroughly with the
156 extracted total cell protein samples. The mixture was then subjected to rotational agitation and
157 incubated overnight at 4℃ to facilitate the formation of immune complexes. The protein-bound
158 magnetic beads were isolated using a magnetic separation rack, and the supernatant from the
159 heated beads was analyzed through SDS-PAGE and western blot.

160 **Immunofluorescence**

161 The cells were washed three times with pre-chilled PBS (P1020, Solarbio), for 1 minute
162 each time. Subsequently, the cells were incubated at 37°C for 20 minutes in an immunostaining
163 fixation solution (P0098, Beyotime) and then underwent three additional washes with PBS,
164 each lasting 5 minutes. Following a 25-minute incubation at room temperature in an
165 immunostaining permeabilization solution (Triton X-100, P0096, Beyotime), the cells were
166 again washed three times with PBS for 5 minutes each. Next, the cells were permeabilized, and
167 non-specific sites were blocked using an immunostaining blocking solution (P0102, Beyotime)
168 at room temperature for 1 hour. The primary antibodies, diluted in an immunostaining primary
169 antibody dilution solution (P0103, Beyotime), were then incubated overnight at 4°C. On the
170 following day, the primary antibodies were removed, and a wash with immunostaining washing
171 solution (P0106, Beyotime) was performed on the cells. Subsequently, the cells were incubated
172 at room temperature for 1 hour with secondary antibodies, diluted in an immunostaining
173 secondary antibody dilution solution (P0108, Beyotime). The cells were washed three times
174 with PBS. Finally, the cells were mounted onto slides using a fluorescence decay mounting
175 medium containing DAPI (S2110, Solarbio). Confocal microscopy images were captured,
176 processed using a laser scanning confocal microscope（TCS SP5II, Leica）, and analyzed
177 using ImageJ.

178 **Cellular GFP-ATZ protein clearance rate assessed by flow cytometry**

179 HEK 293 cells expressing GFP-ATZ were transfected with a plasmid for 48 hours. After
180 centrifugation, the cells were resuspended in phosphate-buffered saline and analyzed using
181 FACScan flow cytometry (BD LSR Fortessa X-20) for GFP fluorescence (488-nm laser
182 excitation, 530/30 filter for detection). A total of 3×10^5 cells underwent scanning to exclude
183 cellular debris based on forward and side-angle scatters (FSC and SSC). Cells expressing GFP
184 were gated, and the percentage depletion of GFP-positive cells was calculated relative to the
185 control group. The clearance rate of GFP-ATZ protein is assessed by measuring the average
186 fluorescence intensity. The clearance rate of GFP-ATZ protein is assessed by measuring the
187 average fluorescence intensity.
188

189 **Cycloheximide Chase Analysis**

190 The CHX chase experiments involved a 48-hour cell culture period following plasmid
191 transfection. Protein synthesis was blocked using CHX treatment at a concentration of 100
192 μg/ml. Cells were collected at various time points, lysed with RIPA buffer, and subjected to
193 SDS-PAGE and immunoblotting analysis with specific antibodies for protein detection.

194 **Real-time Quantitative RT-PCR Assay**

195 Total RNA was extracted from GFP-ATZ expression HEK 293 stable cell line using
196 TRIZOL (15596026, Thermo) according to the manufacturer's instructions. A total of 1μg RNA
197 was used for reverse transcription (QIAGEN, 205311). qRT-PCR was performed using gene-
198 specific primers and SYBR Green Real-time PCR Master Mix (Toyobo, Osaka, Japan). The
199 gene expression levels were normalized to β-actin. Real-time PCR and data collection were
200 conducted on a Bio-Rad CFX96 Connect instrument. The primer sequences used for PCR were
201 as follows: *LAMP2A* and *LAMP2B* and *LAMP2C* forward oligo: 5′-GAA GGA AGT GAA CAT
202 CAG CATG-3′，*LAMP2A* reverse oligo：5′-CTC GAG CTA AAA TTG CTC ATA TCC AGC-
203 3′，*LAMP2B* reverse oligo：5′-CAA GCC TGA AAG ACC AGC ACC-3′，*LAMP2C* reverse

204 oligo: 5′-CTC GAG TTA CAC AGA CTG ATA ACC AGT AC-3′，*HSC70*（*HSPA8*）
205 Forward oligo：5′- CAC TTG GGT GGA GAA GAT TTTG-3′，*HSC70*（*HSPA8*）reverse
206 oligo：5′- CTG ATG TCC TTC TTA TGC TTG C-3′，*SERPINA1* forward oligo: 5′-GGC TGA
207 CAC TCA CGA TGAAA-3′, *SERPINA1* reverse oligo: 5′- GTG TCC CCG AAG TTG ACA
208 GT-3′.

209 **Transcriptional analysis**

210 The KFEE pathway and GO term enrichment were perform using the Hiplot Pro, a
211 comprehensive web service for biomedical data analysis and visualization. It involved utilizing
212 the clusterProfiler package (v.4.5.0) in R software (v.4.2.2), as described by Wu et al [14].
213 Hiplot Pro served as the platform for importing and analyzing the data, while clusterProfiler
214 facilitated various bioinformatics analyses. The analysis was carried out by using R software
215 (v.4.2.2) package clusterProfiler (v.4.5.0) through Hiplot Pro (https://hiplot.com.cn/).
216 Enrichment items with corrected $p<0.05$ were considered significantly enriched.
217

218 **Mitochondrial condition measurements**

219 Cellular mitochondrial membrane potential was assessed using the Mitochondrial
220 Membrane Potential Assay Kit (Beyotime, C2001S) with the TMRE dye. The principle of this
221 assay kit is based on the response of TMRE dye to changes in mitochondrial membrane
222 potential within cells. TMRE, a mitochondria-specific fluorescent probe with red fluorescence,
223 exhibits distinct fluorescence signals upon binding to ATP within the mitochondria [15]. Cells
224 were washed three times with chilled PBS and then incubated with TMRE fluorescent dye at
225 37°C for 30 minutes. Fluorescence intensity was measured using fluorescence microscopy and
226 flow cytometry, with an excitation wavelength of 550nm and an emission wavelength of 575nm.

227 **Cell Viability**

228 To assess cell viability, the Cell Titer-Glo® luminescent cell viability assay kit was used.
229 The amount of ATP inside the cells was measured to indicate cellular metabolic activity. The

230 assay measures the luminescent signal produced by the conversion of ATP to adenosine
231 monophosphate (AMP) by the enzyme luciferase[16]. The treated cells were mixed with the
232 reagent and agitated to induce cell lysis. The mixture was then incubated at room temperature
233 to stabilize the luminescent signal. The luminescence intensity was recorded using the BioTek
234 Synergy Neo2 multimode microplate reader.

235 **Statistical analysis**

236 The statistical analysis of the data was performed using GraphPad Prism 9 (GraphPad
237 Software). The experimental data was presented as mean ± SEM. Comparisons between two
238 groups were conducted by unpaired two-tailed Student's t-test for parametric data, and
239 comparisons between multiple groups were conducted by one-way ANOVA. Statistical
240 significance was set at $p<0.05$.*; $p<0.01$.**; $p<0.001$.***; $p<0.0001$.****; NC, no
241 significance.

242

243 **Results:**

244 **CMA influence homeostasis of wide type and Mutant α1-Antitrypsin Z**

245 In CMA, its activity is primarily modulated by changes in the levels of LAMP2A at the
246 lysosomal membrane[3]. To evaluate CMA's influence on ATZ, a stable cell line was created to
247 express GFP-ATZ, which was subsequently transfected with incremental quantities of the
248 LAMP2A-encoding plasmid. This resulted in a dose-dependent diminution of GFP-ATZ
249 protein levels corresponding to the augmented expression of exogenous LAMP2A (Figure 1A,
250 B). Simultaneously, a reduction in the standard CMA substrate GAPDH was observed,
251 suggestive of enhanced CMA activity (Figure 1B).

252 Due to its aggregation-prone properties, the mutant protein ATZ leads to the formation of
253 insoluble protein inclusions[17]. We thus resuspended the cell pellet in cell lysis buffer
254 containing 2% SDS and dissect the CMA's effect on insoluble ATZ. Unlike A1AT, we observed
255 an aberrant amount of ATZ in the insoluble fraction. However, with the expression of LAMP2A,
256 the insoluble ATZ level also significantly reduced (Figure 1C). Additionally, transfecting
257 LAMP2A into the HepG2 hepatic cell line, which naturally expresses A1AT, resulted in a

258 significant decline in endogenous A1AT levels upon LAMP2A overexpression (Figure 1D).
259 This indicates that LAMP2A overexpression disrupts the homeostasis of both wild-type A1AT
260 and ATZ.

261 To further validate the regulatory effect of LAMP2A on ATZ, we attempted to manipulate
262 the endogenous levels of LAMP2A. We designed two short hairpin RNAs (shRNAs) that
263 specifically target the cytosolic tail of the LAMP2A transcript, a region that differs between
264 Lamp2 gene isoforms A and B, C (Supplementary Figure 1A， 1B). After transfecting the cells
265 expressing GFP-ATZ with the two shRNA-coded vectors for 48 hours, a significant (>70%)
266 reduction in LAMP2A mRNA levels was observed compared to cells treated with a scrambled
267 shRNA, while no noticeable changes were detected in the transcripts of LAMP2B and
268 LAMP2C (Supplementary Figure 1C,1D). Moreover, in the same samples, we detected a
269 notable increase in GFP-ATZ protein levels (Figure 1E, 1F).

270 As the modulation of LAMP2A did not alter ATZ transcription (Supplementary Figure
271 2A), we speculate that the changes in ATZ levels may result from altered protein degradation
272 dynamics. To confirm this, we blocked protein synthesis in the ATZ expression cells with
273 cycloheximide (CHX) 24 hours after LAMP2A coding plasmids transfection and monitored the
274 remaining ATZ at different time points post the drug treatment. The results indicated an
275 accelerated degradation of ATZ in cells with LAMP2A overexpression, as evidenced by a
276 decrease in half-life from 8 to 6 hours (Figure 1G). Additionally, overexpression of HSC70,
277 another key component of CMA[4], also heightened the degradation of GFP-ATZ in a dose-
278 dependent manner(Supplementary Figure 3A、B). These experiments collectively suggest that
279 CMA plays a significant role in the proteostasis of both mutant ATZ and wild-type A1AT.

280 **ATZ is degraded through the CMA pathway mediated by LAMP2A**

281 The above assays have provided evidences supporting CMA's participation in regulating
282 ATZ's degradation, and we hypothesize that CMA directly targets ATZ for clearance. To
283 corroborate this hypothesis, we conducted a pull-down assay of ATZ-flag protein and confirmed
284 the association with LAMP2A (Figure 2A). Additionally, we stained endogenous LAMP2A and
285 examined its co-localization with ATZ. We observed distinct CMA puncta, as indicated by

286 LAMP2A, and a significant overlap between GFP-ATZ and LAMP2A (Figure 2B). We also
287 examined the interaction between ATZ and HSC70 and found a potent binding of ATZ with
288 HSC70 (Supplementary Figure 3C).

289 The degradation of substrates by CMA relies on the acidic environment within lysosomes
290 [18]. To investigate whether ATZ degradation is dependent on the lysosome, we treated cells
291 overexpressing LAMP2A with lysosomal inhibitor chloroquine (CQ) for variable times. We
292 observed that the level of CQ blocked the autophagic-lysosomal pathway, leading to
293 accumulated levels of ATZ (Figure 2D). These evidences thus prove the directed accessibility
294 of CMA to ATZ and its mediation of degradation depending on lysosomal hydrolysis activity.
295 Consistent with this, we found that QX77[19], a CMA-specific activator, was able to boost
296 LAMP2A's level and eliminate the typical CMA substrate GAPDH, as well as GFP-ATZ
297 (Figure 2E).

298 The cytosolic tail of LAMP2A, comprising 12 amino acids, is essential for the recruitment
299 of HSC70-substrate complexes to lysosomes, facilitating their interaction via positively
300 charged residues [20,21]. To elucidate how LAMP2A recognizes ATZ, we engineered plasmids
301 for two LAMP2A variants: one encoding a truncated version lacking the C-terminal tail
302 (LAMP2A-truncate), and another encoding a mutant wherein positively charged amino acids
303 at positions 401 to 404 (401KHHH404) were substituted with alanines (401AAAA404) (Figure
304 2F，Supplementary Figure 4). These plasmids were introduced into cells expressing GFP-ATZ.
305 Our findings revealed that only the wild-type LAMP2A significantly reduced ATZ levels,
306 whereas both the LAMP2A-truncate and LAMP2A-mutant variants were ineffective (Figure
307 2G). Additionally, immunoprecipitation assays with Flag-tagged ATZ demonstrated markedly
308 reduced co-immunoprecipitation with the truncated and mutant forms of LAMP2A (Figure 2H).
309 These data further affirm that CMA facilitates ATZ degradation in a LAMP2A-dependent
310 manner, highlighting the critical role of the C-terminal cytosolic tail in mediating this
311 interaction.

312 **The 121QELLR125 pentapeptide motif is crucial in CMA mediated ATZ degradation**

313 The CMA pathway differs from autophagy in its distinct substrate preference. Substrates

314 degraded through the CMA pathway typically contain the classical "KFERQ" pentapeptide
315 sequence, which serves as a recognized site by HSC70[3]. Using the "KFERQ finder V0.8"
316 web server (https://rshine.einsteinmed.edu/), we identified a typical KFERQ motif
317 (121QELLR125) within the ATZ protein. To investigate the role of this specific motif, we
318 engineered a mutant variant, AA-ATZ (121AALLR125) (Figure 3A) and evaluated its binding
319 affinity to HSC70 and LAMP2A through a CO-IP assay. Remarkably, the mutant demonstrated
320 a marked decrease in binding to both LAMP2A and HSC70 compared to the ATZ protein
321 (Figure 3B, 3C). Immunofluorescence assays further substantiated the diminished interaction
322 between the mutant ATZ protein and LAMP2A (Figure 3D).

323 In addition, we observed that the basal protein level of AA-ATZ was significantly higher
324 than that of ATZ under the condition of equal transfection of ATZ or AA-ATZ plasmids,
325 regardless of whether LAMP2A was overexpressed or not (Figure 3E). We hypothesized that
326 this discrepancy was caused by the inefficient degradation of mutant AA-ATZ by CMA. To
327 prove this, we compared the degradation rate of ATZ with that of AA-ATZ under conditions of
328 high CMA activity with a CHX chasing experiment. The results showed that, indeed, with the
329 activation of CMA, the degradation rate of AA-ATZ was slower than ATZ, with a protein half-
330 life reduced from 5.2 hours to 3.5 hours (Figure 3F). These results underscore the importance
331 of the CMA pentapeptide 121QELLR125 in ATZ for its degradation through the CMA pathway.
332 They further demonstrate that ATZ is *bona fide* substrate of CMA.

333 **CMA degrade ATZ independent of macroautophagy**

334 With above assays, we confirmed that ATZ could be degraded via the CMA pathway.
335 However, there are complicated compensatory regulatory mechanisms between
336 macroautophagy and CMA [22-24]. To mitigate the influence of macroautophagy, we employed
337 autophagy-deficient HeLa *ATG16L1-/-* cells[25] to reassess our findings. In wild-type HeLa
338 cells, we observed that serum starvation not only activates CMA but also macroautophagy, as
339 indicated by increased levels of LAMP2A and LC3II, alongside enhanced ATZ degradation
340 (Figure 4A). Conversely, in HeLa *ATG16L1-/-* cells subjected to identical starvation conditions,
341 the absence of LC3II formation confirmed the disruption of autophagy, yet ATZ protein levels

342 still diminished (Figure 4B). Furthermore, in HeLa *ATG16L1*-/- cells, the overexpression of
343 exogenous LAMP2A resulted in dose-dependent degradation of ATZ, which was similarly
344 effective in wild-type alpha-1 antitrypsin A1AT and insoluble ATZ aggregates (Figures 4C, D).
345 By employing CMA-specific activators, AR7 and QX77 [26,27], we noted identical
346 degradation patterns for the prototypical CMA substrates GAPDH and ATZ (Figure 4E).
347 Further investigations into the pentapeptide's influence in autophagy-deficient cells showed that
348 AA-ATZ exhibited a lower degradation efficiency than ATZ (Figure 4F). These data suggesting
349 that CMA is capable of degrading ATZ independently of macroautophagy.

350 In addition to its role in autophagy, *ATG16L1* has been implicated in anti-inflammatory
351 responses and the regulation of hormone secretion[28,29]. To rule out the influence of
352 *ATG16L1*'s non-autophagic functions, we utilized another autophagy deficient model, the HeLa
353 *BECLIN 1-/-* cell line [30,31]. In the HeLa *BECLIN* 1-/- cells, a similar decrease in ATZ protein
354 levels was observed after inducing CMA through serum starvation and LAMP2A
355 overexpression (Figure 4G, H). Notably, this decline in ATZ persisted despite the inhibition of
356 the proteasome pathway when LAMP2A was overexpressed (Figure 4H). These findings lend
357 further support to the notion that CMA can independently facilitate the degradation of ATZ.

358 **CMA-mediated ATZ degradation mitigates cellular stress**

359 Prior research indicates that ATZ aggregates leads to the cellular toxicity including
360 mitochondrial damage[32]. We conducted a comparison of cell survival rates under normal
361 conditions and after activating CMA. Overexpression of LAMP2A and HSC70 in cell lines
362 stably expressing GFP-ATZ significantly improved cell viability (Figure 5A).Mitochondrial
363 membrane potential alterations serve as a critical metric for mitochondrial damage assessment
364 [33]. Using the TMRE probe to measure mitochondrial inner membrane potential[15], a notable
365 increase in fluorescence intensity was detected upon overexpression of LAMP2A and HSC70,
366 as compared to controls (Figure 5B,5C). This enhancement suggests a reestablishment of
367 mitochondrial integrity, implicating the potential of CMA activation in mitigating
368 mitochondrial damage.

369 Through transcriptome-wide analysis, we found that CMA activation via LAMP2A

370 overexpression results in the upregulation of three genes and the downregulation of sixteen
371 genes (Figure 5D, Supplementary Table). Notably, genes implicated in apoptosis and oxidative
372 protein damage, such as DNAJB1, HSPA6, ANKRD1, and EDEM2, were markedly
373 downregulated. Gene Ontology (GO) enrichment analysis further suggested that these
374 downregulated genes are predominantly associated with chaperone-mediated protein folding
375 (Figure 5E, Supplementary Figure 5). Additionally, KEGG pathway analysis underscored the
376 downregulated genes' roles in protein processing in the endoplasmic reticulum (ER)
377 (Supplementary Figure 5). Considering the established function of heat shock proteins (HSPs)
378 in the management of protein misfolding and ER stress, we performed a cluster analysis of HSP
379 genes related to protein misfolding. The analysis revealed a decrease in the expression of
380 various HSP genes upon CMA activation (Figure 5F), suggesting that enhanced ATZ
381 degradation through CMA may alleviate ER stress and diminish the necessity for protein
382 chaperones.
383
384 **Discussion**
385 A comprehensive understanding of the catabolic mechanism responsible for the
386 degradation of ATZ is essential for advancing therapeutic strategies for AATD. To date, the
387 degradation of ATZ has been associated with both the proteasome and autophagy-lysosome
388 pathways[34]. Multiple evidences indicated upregulated autophagic pathway in the AATD
389 pathologic cells, and augmentation of autophagy has been demonstrated to facilitate the
390 clearance of ATZ aggregates [11,35]. Furthermore, recent evidence has identified a
391 noncanonical ER-to-lysosome-associated degradation pathway (ERLAD) that transports ATZ
392 directly from the ER to the lysosome[36]. Despite this, the specific role of CMA in ATZ
393 catabolism remains to be fully elucidated. This study presents biochemical evidence confirming
394 CMA's role in ATZ degradation and elucidates its underlying mechanisms.
395 CMA is a selective process where the chaperone protein HSC70 recognizes misfolded
396 proteins, delivering them to LAMP2A for internalization. [37]. Our first piece of evidence
397 supporting the involvement of CMA in the regulation of ATZ comes from the finding that
398 LAMP2A directly interacts with ATZ and promotes its degradation (Figure 1 and 2). LAMP2A,
399 produced by alternative splicing of the LAMP2 gene, is the only isoform implicated in CMA

400 [38,39]. The selective silencing of LAMP2A leads to increased ATZ levels, underscoring
401 CMA's unique role in managing ATZ (Figure 1).

402 The structural distinctions between LAMP2 isoforms are localized to their C-terminal
403 transmembrane region and cytoplasmic tail. The cytoplasmic tail's positively charged residues
404 are vital for substrate recognition in CMA [39]. Our research demonstrates that alterations to
405 the cytoplasmic tail, either through deletion or modification of these key amino acids,
406 compromise substrate binding and consequently hinder degradation (Figure 2G, H). This
407 corroborates previous research underscoring the critical role of the cytoplasmic tail in the
408 recognition of substrates by the CMA pathway.

409 CMA specific pentapeptide KFERQ motif in substrate is absolutely necessary for CMA
410 mediated degradation, because it serves as a recognition site for HSC70 binding [40]. In this
411 study, we identified a pentapeptide sequence, 121QELLR125, on ATZ and demonstrated that
412 modifications to this sequence significantly weaken the interactions among ATZ, HSC70, and
413 LAMP2A (Figure 3B, C). Variants of ATZ lacking this motif displayed a marked decrease in
414 degradation rate, resulting in significant accumulation, even under normal physiological
415 conditions (Figure 3E, F). The identification of 121QELLR125 motif further confirm ATZ as a
416 bona fide substrate for CMA.

417 Macroautophagy and CMA, both lysosomal-dependent digestion pathways, are
418 coordinately regulated in response to stress, with complex interplay and compensatory
419 mechanisms. For example, the activation of CMA has been observed to suppress
420 macroautophagy, while blocking CMA triggers an upregulation of macroautophagy [22,24].
421 Conversely, the induction of macroautophagy has been shown to diminish CMA activity [23].
422 In our study, we utilized two different autophagy-deficient cell lines to confirm that CMA acts
423 independently to degrade ATZ (Figure 4). Conventionally, it is believed that in AATD affected
424 cells, soluble ATZ is degraded by the proteasome system [10], whereas insoluble aggregates
425 are cleared by autophagy-lysosome pathways and the ERLAD pathway[11,35,36]. The
426 identification of CMA as a novel pathway for ATZ clearance brings us closer to achieving a
427 comprehensive understanding of the catabolic processes involved in ATZ metabolism.

428 Microautophagy is another cellular degradation pathway conserved in mammalian cells,
429 characterized by the direct engulfment of substrates by invagination of the lysosomal

membrane[41]. The available data allow us to conclude that ATZ is a substrate of CMA, as it meets all the criteria for CMA substrates, including possessing the KFERQ-like pentapeptide, interacting with HSC70 and LAMP2A, and undergoing digestion within the lysosome. But it also raises another question: what is microautophagy's role in ATZ's catabolic regulation? While the precise involvement of microautophagy remains to be conclusively determined, emerging evidence suggests it could play a role in modulating ATZ levels. For example, overexpression of HSC70 exerts a greater effect on the clearance of ATZ and overall cellular recovery than LAMP2A overexpression does (Figure 5A). Such an effect is consistent with the process of endosomal microautophagy (e-MI), which selectively engulfs soluble proteins that present a KFERQ-like pattern, with HSC70 facilitation[42]. We postulate in that case overexpressed HSC70 may redirect a portion of ATZ to e-MI for degradation, offering additional cellular protection. Extensive research is necessary to thoroughly elucidating these mechanisms in this regard.

ER stress and mitochondrial damage are two typical characteristics of ATZ-induced cellular malfunctions[43,44]. In our study, we observed simultaneous alleviation of mitochondrial damage and restoration of cellular growth status upon the effective activation of CMA. Transcriptomic analysis revealed that CMA activation marginally altered global gene expression, with only 16 genes showing significant downregulation. Of these, four were intimately linked to protein folding, suggests a rebalancing of proteostasis due to the reduced presence of intracellular misfolded proteins [45]. The diminished expression of EDEM2, a gene implicated in endoplasmic reticulum-associated protein degradation [46], hints at the successful removing of misfolded proteins from the ER and a reduction in ER stress. Moreover, notable decreases in the expression of DNAJB1 and ANKRD1 both associated with apoptotic regulation[47] and ANKRD1[48], suggesting reduced cell apoptosis further confirming the positive role played by CMA towards maintaining cellular viability (Figure 5).

However, it is important to note that CMA serves as an essential intracellular protein degradation pathway. In theory, CMA targets proteins containing the KFERQ motif, which accounts for approximately 30% of soluble cytosolic proteins. Enhancing CMA activity would facilitate the removal of misfolded and oxidized proteins, and ultimately enhancing cellular viability[22]. Hence, in this context, Thus, the observed cellular recovery should not be

460 exclusively credited to ATZ aggregate removal but also acknowledged as a broader impact of
461 CMA in reducing general cellular stress by targeting various oxidized and misfolded proteins.
462 The aggregation of ATZ is a major contributor to the pathogenesis of AATD liver disease,
463 prompting various attempts to halt or reverse the aggregation process and mitigate AATD
464 progression. These strategies include inhibiting ATZ synthesis[49-51], enhancing secretion
465 [52,53], blocking polymerization [54,55] and promoting degradation [35,56]. The identification
466 of macroautophagy activation as a means to accelerate ATZ degradation has led to the
467 investigation of autophagy-boosting drugs such as carbamazepine, rapamycin, and
468 fluphenazine[12]. Our discovery of CMA involvement in the regulation of ATZ suggests that
469 specific enhancers of CMA may offer new therapeutic options for AATD. Since the discovery
470 of CMA pathway, there have been many attempts to discover small molecules for CMA
471 manipulation. In recent years, a series of small molecular drugs that can activate CMA have
472 been found. However, most CMA activators interfere with other cellular pathways, often
473 causing disturbance in essential cellular processes, including biomaterial metabolism or protein
474 synthesis, which hinders their application[57]. AR7 and QX77 both derivatives of retinoic acid,
475 stands out as the most effective CMA inducer developed thus far [19,27].
476 In our model, we found the treatment with AR7 and QX77, enhancing CMA activity and
477 clearing ATZ in both normal and autophagy-deficient cells (Figure1E and 4E). This finding
478 suggests that CMA-specific activators could serve as potential small-molecule drug therapies
479 for AATD. Previous studies conducted with Alzheimer's disease mice have also demonstrated
480 the clearance of pathological proteins when treated with AR7 derivatives, thereby providing
481 support for their potential therapeutic implications [58]. Thus, performing future in vivo studies
482 to investigate the impact of these CMA activators on ATZ clearance in animal models would
483 hold significant value, allowing us to gain a deeper understanding of their therapeutic potential.
484 In conclusion, our study establishes CMA as a previously neglected protein degradation
485 pathway involved in regulating the catabolism of ATZ. As depicted in Figure 6, in addition to
486 the proteasome and autophagy, ATZ can also undergo degradation via CMA. Specifically, the
487 ATZ protein is recognized by HSC70 through the pentapeptide 121QELLR125 and delivered
488 to LAMP2A to interact with its C terminal cytosolic tail on the lysosomal membrane, the
489 LAMP2A then transporting the substrate into the lysosome for digestion. Activation of CMA,

either through the overexpression of LAMP2A or the use of small molecular activators, enhances the digestion of ATZ, thereby slowing down its aggregation process and mitigating cellular stress.

Figure

Figure 1: LAMPA2A influence mutant alpha one antitrypsin ATZ steady-state protein level

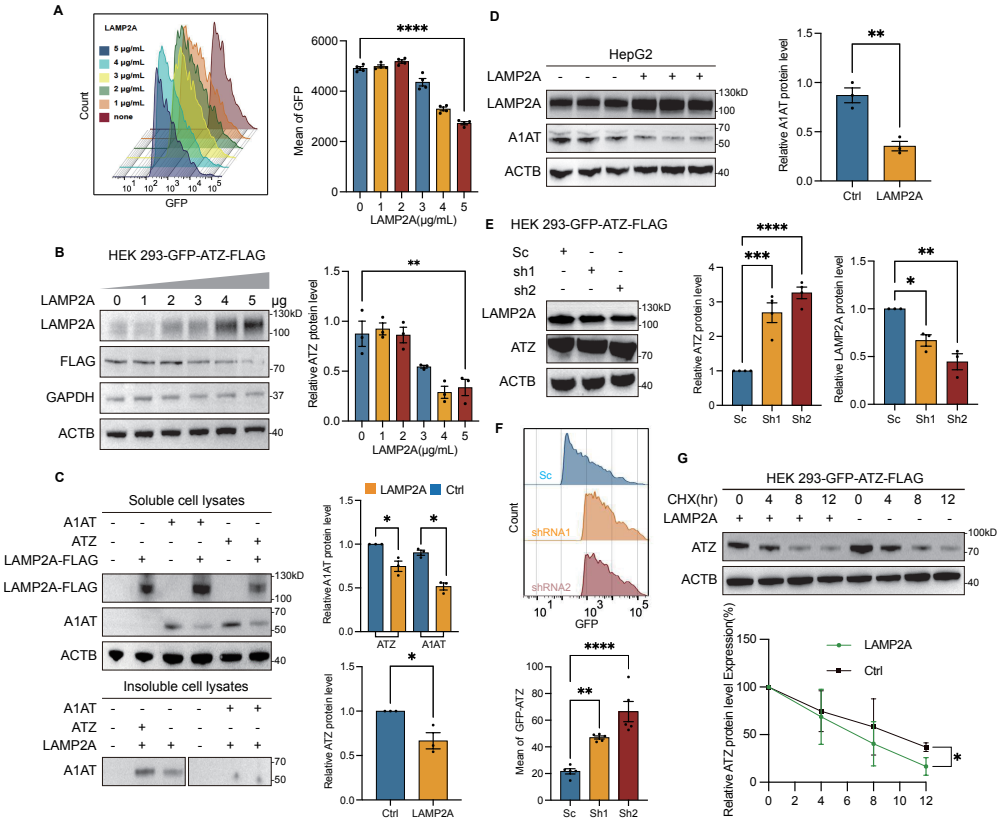

A: GFP-ATZ-expressing HEK 293 cells were transfected with increasing amounts (1, 2, 3, 4, or 5 μg/mL of cell medium) of a vector expressing LAMP2A for 48 hours. The fluorescence of GFP-ATZ was analyzed by flow cytometry.

B: HEK 293 cells were transfected with increasing concentrations (1, 2, 3, 4, or 5 μg/mL of cell medium) of vectors expressing LAMP2A for 48 hours. The protein levels of GFP-ATZ relative to LAMP2A in cell lysates were quantitatively analyzed by measuring densitometry values from the blots.

C: HEK 293 cells were co-transfected with LAMP2A and either ATZ or A1AT. After 48 hours, the cells were lysed using 0.1% Triton X-100 as a detergent, and the lysates were divided into Triton X-100 soluble cell lysates and Triton X-100 insoluble cell pellet fractions. Equal aliquots of cell lysates (30 μg) were loaded onto SDS-PAGE and immunoblotted with

536 antibodies against ATZ and LAMP2A. Ctrl: pCDH empty plasmid.

537 D: HepG2 cells were transfected with empty or LAMP2A-expressing vectors. After 48
538 hours of transfection, cell lysates were harvested and immunoblotted with the indicated
539 antibodies.

540 E: HEK 293 cells stably expressing GFP-ATZ were transfected with shRNA1 or shRNA2
541 to knock down LAMP2A protein expression for 48 hours. The levels of GFP-ATZ protein from
542 different cells were quantitatively analyzed. Cells transfected with non-targeted scramble-
543 shRNA were used as the control. Ctrl: scramble shRNA, sh1: LAMP2A-shRNA1, sh2:
544 LAMP2A-shRNA2.

545 F: HEK 293 cells stably expressing GFP-ATZ were transfected with shRNA1 or shRNA2
546 to knock down LAMP2A protein expression for 48 hours. The fluorescence of GFP-ATZ was
547 analyzed by flow cytometry.

548 G: GFP-ATZ-expressing HEK 293 cells were transfected with empty or LAMP2A-
549 expressing vectors. Cells were treated with cycloheximide (CHX; 10 μg/mL) for the indicated
550 times, starting 24 hours after transfection. The graph illustrates the quantitative changes in
551 steady-state levels of GFP-ATZ relative to actin during the CHX treatment period.

552 Data were presented as the mean ± SEM of 3 or more independent experiments. $p<0.05$.*;
553 $p<0.01$.**; $p<0.001$.***; $p<0.0001$.****; NC, no significance. vs. indicated group.

554
555
556
557
558
559
560
561
562
563
564
565

Figure 2: ATZ undergoes degradation via the CMA pathway facilitated by LAMP2A

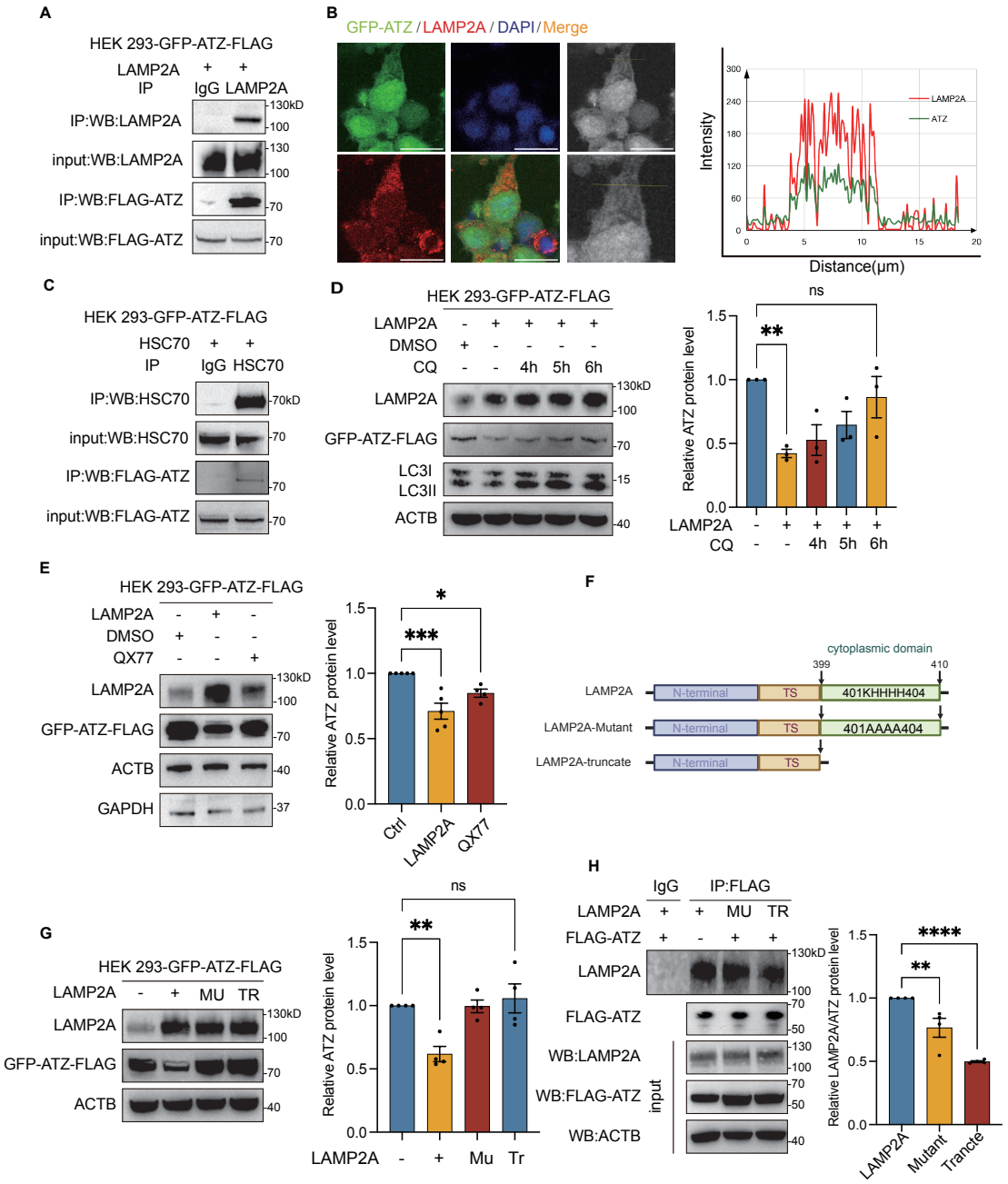

A、C:HEK 293 stably expressing GFP-ATZ were transfected with an empty vector and LAMP2A or HSC70 for 48 hours, cells were lysed and subjected to immunoprecipitation with antibodies against IgG or Flag. Aliquots of IP proteins and input proteins were analyzed by immunoblot.

B：HEK 293 stably expressing GFP-ATZ (green) were transiently transfected with

HSC70 or LAMP2A for 48 h. Immunofluorescence microscopic images of GFP-ATZ (green) and LAMP2A(red) in HEK 293 stably expressing GFP-ATZ cells were obtained after staining with anti-LAMP2A antibodies. Each nucleus was stained with DAPI (blue). The co-localization of LAMP2A and ATZ-GFP were visualized as yellow color caused by superimposing of red and green. Plots of pixel intensity along the white line rows of images to the left of each plot, colors as in merged images. Scale bars: 10 μm

D: GFP-ATZ-expressing HEK 293 cells were transfected with an empty vector or a vector encoding LAMP2A for 36 hours. Subsequently, they were treated with CQ (10μM) for an additional duration of 4, 5, or 6 hours. Following the treatment, the cells were lysed and underwent western blot analysis.

E: HEK 293 cells expressing GFP-ATZ were treated with DMSO or QX77 (10μM) for 48 hours. Cell lysates were immunoblotted with the indicated antibodies.

F: Schematic depiction of a full-length LAMP2A construct and LAMP2A-mutant construct. TS：Transmembrane structure.

G: GFP-ATZ-expressing HEK 293 cells were transfected with full-length LAMP2A, LAMP2A-mutant, or LAMP2A-truncate constructs for 48 hours. The protein levels of GFP-ATZ in different transfections were quantitatively analyzed. TR: LAMP2A truncate, Mu: LAMP2A mutant.

H: HEK 293 cells were transfected with LAMP2A, LAMP2A-mutant, or LAMP2A-truncate along with FLAG-ATZ for 24 hours. The cell lysates were then subjected to immunoprecipitation (IP) using an anti-Flag antibody, and the precipitates were analyzed by western blotting. TR: LAMP2A truncate, MU: LAMP2A mutant.

Data were presented as the mean ± SEM of 3 or more independent experiments. $p<0.05$.*; $p<0.01$.**; $p<0.001$.***; $p<0.0001$.****; NC, no significance. vs. indicated group.

Figure 3: Pentapeptide 121QELLR125 on ATZ is critical in CMA mediated degradation

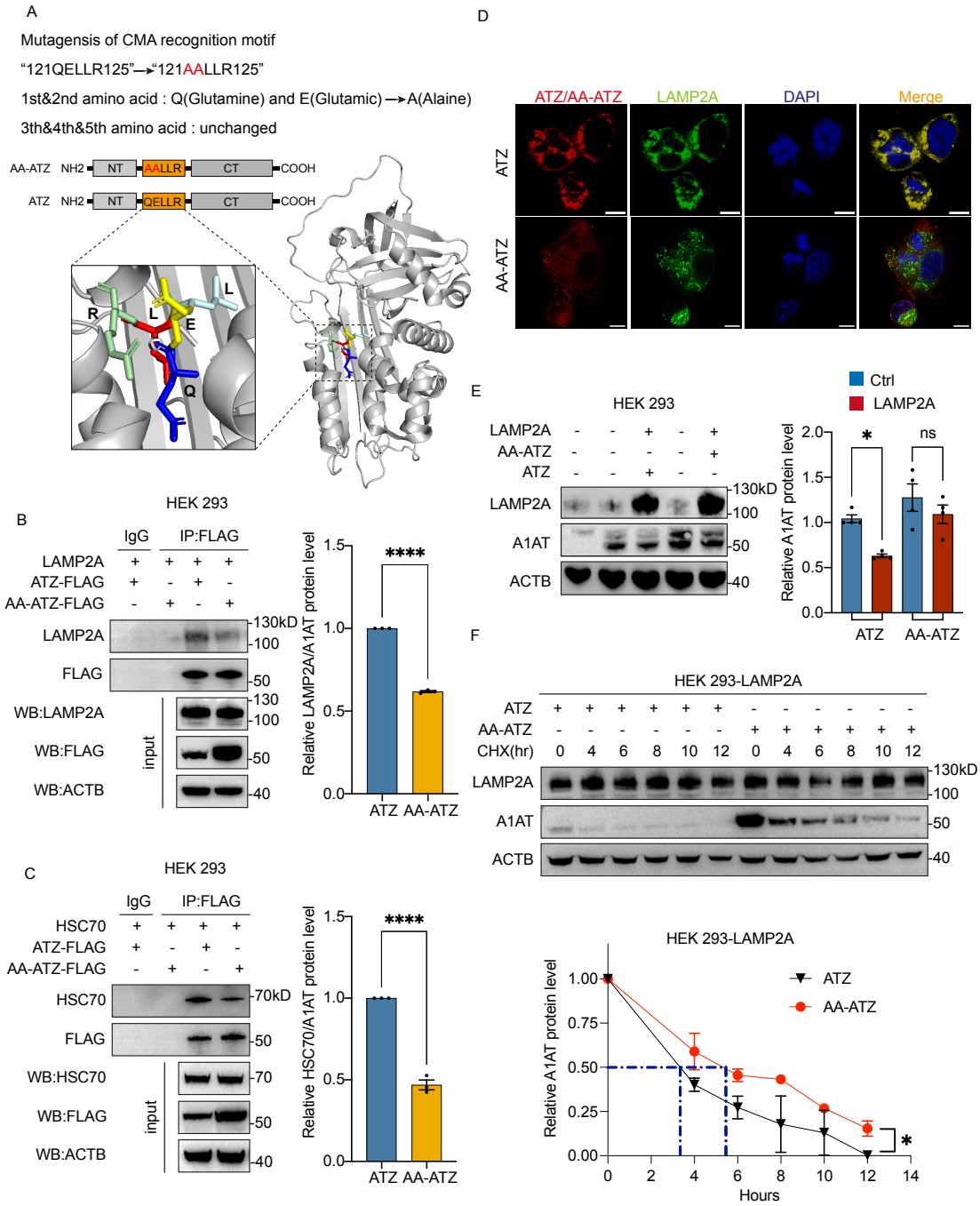

A: The cartoon illustrates the structure of alpha-1 antitrypsin, with the pentapeptide sequence (121QELLR125) highlighted in orange. The combined ribbon representation and stick model showing the overall structure and the CMA motif of ATZ protein. This model was generated using PyMOLTM based on the Protein Data Bank code 3CWM.

B、C:HEK 293 cells transfected with LAMP2A or HSC70 and ATZ-FLAG or AA-ATZ-

612 FLAG for 48h. Lysates were immunoprecipitated (IP) with either IgG, anti-LAMP2A antibody
613 and probed for ATZ-FLAG, AA-ATZ-FLAG and LAMP2A or HSC70.
614 D: HEK 293 cells were con-transfected for 48 hours with LAMP2A expressing vectors or
615 vector coding wide type ATZ or AA-ATZ mutant. Representative confocal images showing the
616 colocalization of ATZ-FLAG (red) or AA-ATZ-FLAG (red) and LAMP2A(green) in HEK 293T
617 cells. Scale bars: 10 μm
618 E: HEK 293 cells were co-transfected with LAMP2A expressing vectors or vectors
619 encoding wild-type ATZ or AA-ATZ mutant for 48 hours. The cells were lysed, and western
620 blot analysis was conducted to assess the expression of GFP-ATZ.
621 F: HEK 293 stably expressing LAMP2A cells were transfected with wide type ATZ or AA-
622 ATZ expressing vectors. The transfected cells were cultured for 24 h before being further
623 incubated with cyclohexamide (CHX;10 μg/ml) for the indicated time. The levels of A1AT at
624 different time points were detected by Western blot.
625
626
627
628
629
630
631
632
633
634
635
636
637
638
639
640
641

Figure 4: ATZ was a bona fide substrate of CMA. Ectopic expression of Lamp2A in macro-autophagy deficient cell causes reduction of ATZ

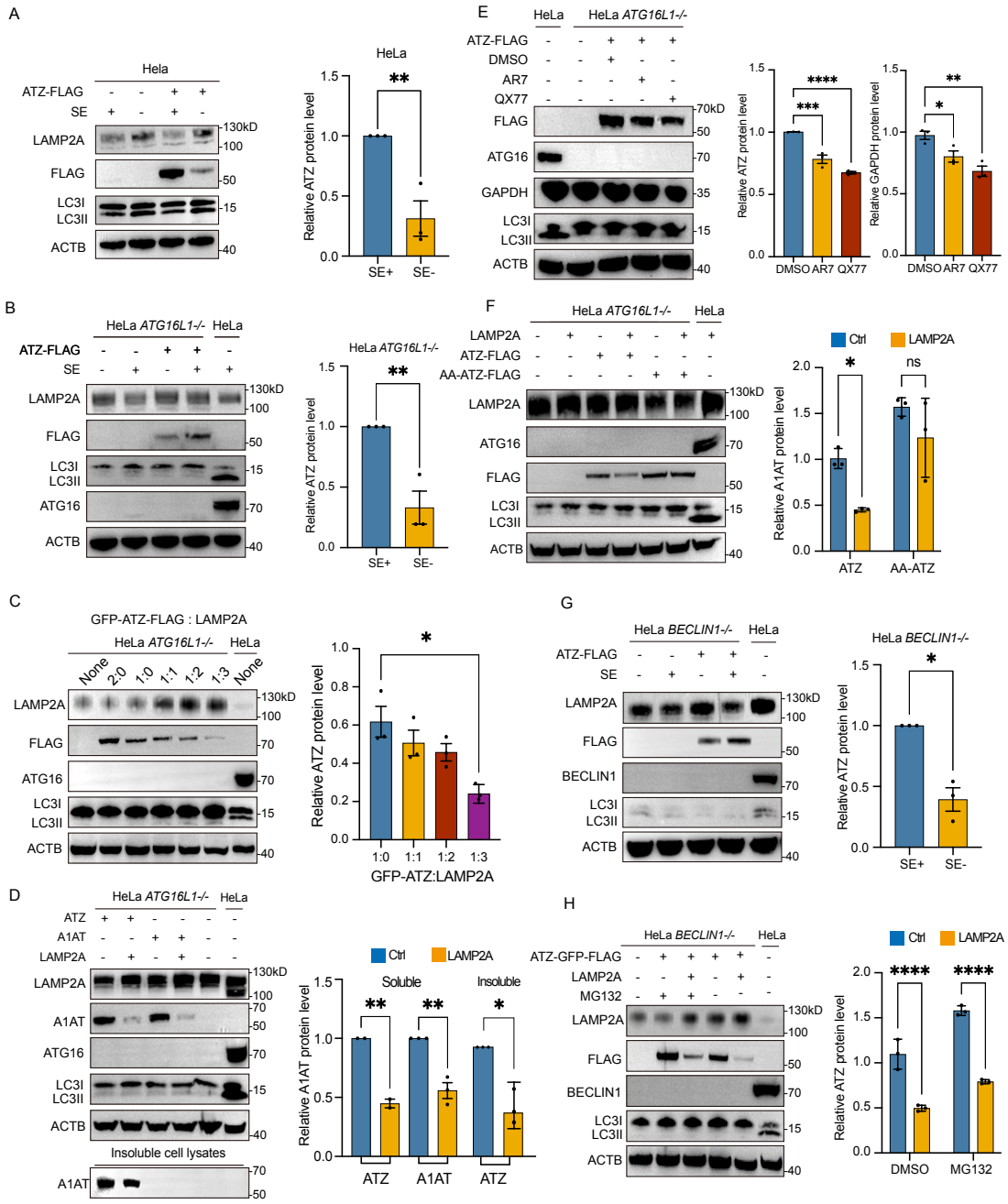

A: Hela *ATG16L1-/-* cells were transfected with ATZ-GFP-FLAG and amounts of a LAMP2A or expressing vector. Cells were lysed for Western analysis.

B: HeLa *ATG16L1-/-* cells were transfected with LAMP2A and ATZ-FLAG or A1AT vectors. After 48 hours, cells were lysed using 0.1% Triton X-100 as a detergent, and the lysates were fractionated into Triton X-100 soluble cell lysates(n=2) and Triton X-100 insoluble cell

pellet fractions(n=3). Equal amounts of cell lysates (30 g) were loaded onto SDS-PAGE and subjected to immunoblotting using antibodies against ATZ and LAMP2A.

C: HeLa *ATG16L1-/-* transfected with FLAG-ATZ for 36h，treated with QX77(10μM) or AR7(10μM) for 24h, cell lysates were harvested and immunoblot with the indicated antibodies.

D、E、F: Transfection of the ATZ-FLAG plasmid was performed in HeLa, HeLa *ATG16L1-/-*, and HeLa *BECLIN1-/-* cells. After 48 hours, the cells were subjected to free DMEM for 24 hours, followed by lysis of the cells for immunoblotting analysis.

G: HeLa *BECLIN1-/-* cells were transfected with ATZ-FLAG and an Empty vector or LAMP2A for 36 hours and then treated with MG132 (20 μM) for an additional 4 hours. Cells were lysed and subjected to Western blot analysis.

H: Immunoblotted assay of HeLa *ATG16L1-/-* cells transfected with LAMP2A and ATZ-FLAG or AA-ATZ-FLAG mutant.

Data were presented as the mean ± SEM of 3 or more independent experiments. $p<0.05$.*; $p<0.01$.**; $p<0.001$.***; $p<0.0001$.****; NC, no significance. vs. indicated group.

Figure 5: The degradation of ATZ facilitated by CMA alleviates cellular distress and ameliorates cellular states.

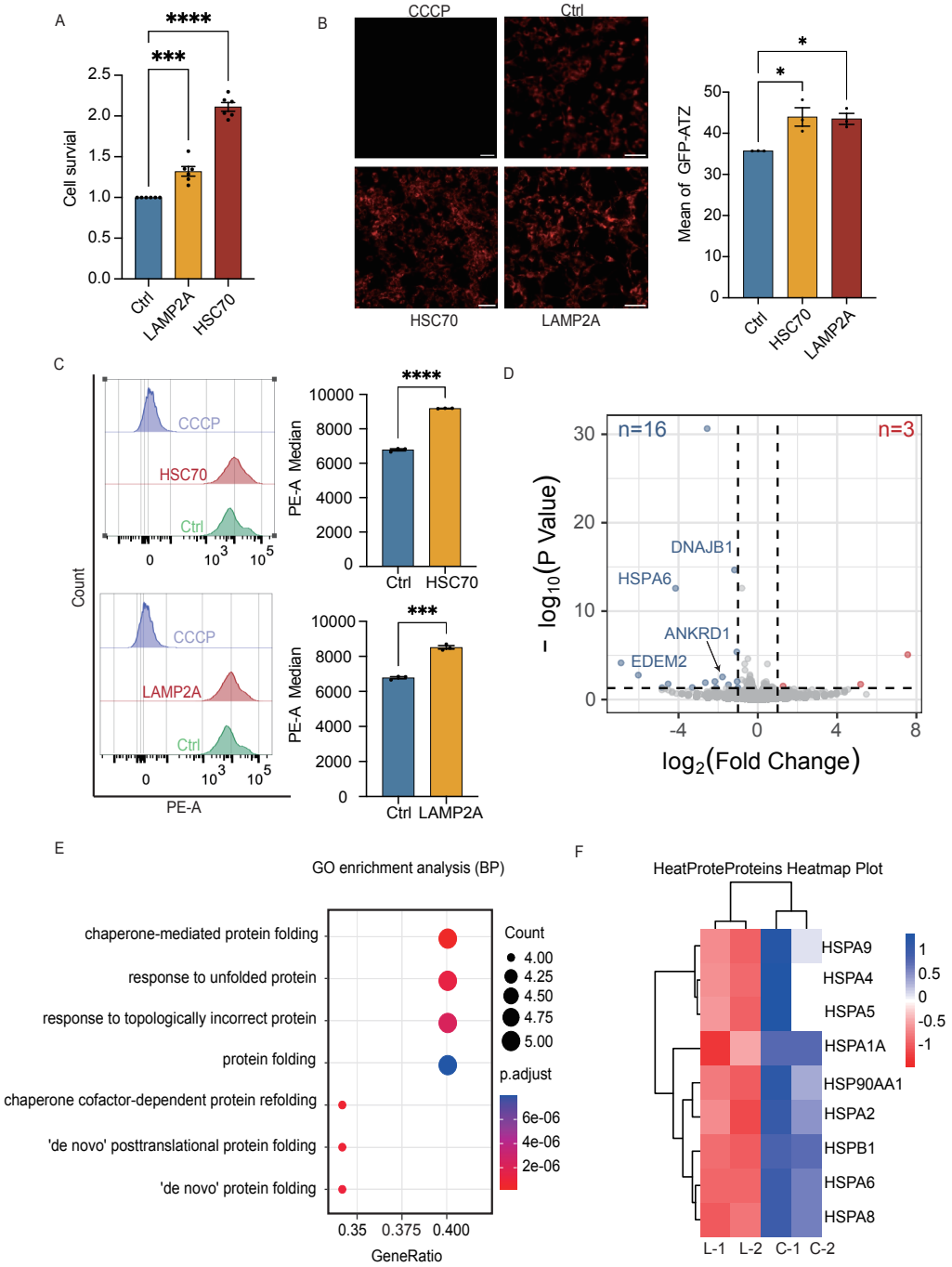

A: HEK 293 cells expressing GFP-ATZ were transfected with LAMP2A or HSC70 for 48 hours. Cell viability analysis was performed using the CellTiter-Glo luminescent cell viability assay.

B: TMRE signals in HEK 293 cells expressing GFP-ATZ were detected by fluorescence

microscopy. Scale bars: 50 μm. CCCP: negative control. Ctrl：pCDH empty plasmid.

C: HEK 293 cells expressing GFP-ATZ were transfected with either LAMP2A or HSC70, then stained with TMRE or CCCP for flow cytometry analysis. CCCP: negative control. Ctrl：pCDH empty plasmid.

D: A volcano plot was generated to compare the log2 fold change (logFC) versus the p-value between control cells and LAMP2A-expressing cells. Grey circles represent RNAs with a p-value > 0.05, blue circles represent downregulated RNAs with a p-value < 0.05 and fold change greater than 2, while red circles represent upregulated RNAs with a p-value < 0.05 and fold change greater than 2, n=2.

E: The expression levels of 16 genes displaying downregulation in HEK 293-GFP-ATZ cells under LAMP2A transfection conditions were subjected to Gene Ontology (GO) functional enrichment analysis (Biological Process).

F: The corresponding heatmap highlights the disparity in RNA expression levels related to the heat shock protein family between the overexpression of the LAMP2A plasmid and the empty vector in GFP-ATZ-expressing HEK 293 cells.

Figure 6: The schematic diagram illustrates the degradation mechanism of ATZ through the CMA pathway

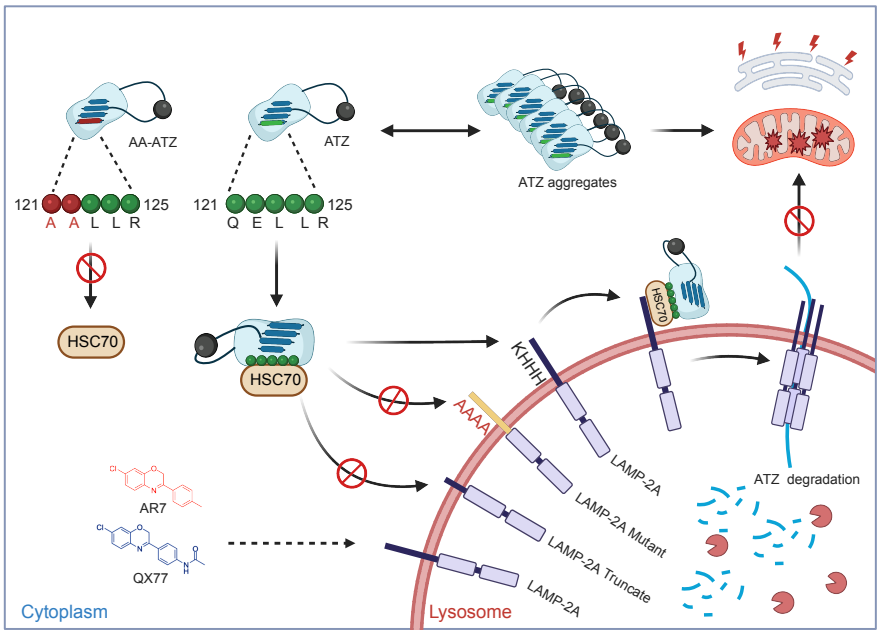

Besides proteasome and autophagy pathways, CMA also plays a role in alpha-1 antitrypsin Z (ATZ) degradation. Specifically, the heat shock cognate 70 (HSC70) protein recognizes the ATZ protein through the pentapeptide sequence 121QELLR125 and transports it to lysosome-associated membrane protein 2A (LAMP2A) on the lysosomal membrane. Augmenting CMA activity through LAMP2A overexpression or AR7 utilization enhances ATZ digestion via this pathway, thereby alleviating cellular stress, including ER stress and mitochondrial impairment.

738 **Reference:**

739 1. Cuervo AM. Autophagy: in sickness and in health. Trends Cell Biol. 2004
740 Feb;14(2):70-7.
741 2. Mizushima N, Ohsumi Y, Yoshimori T. Autophagosome formation in mammalian
742 cells. Cell Struct Funct. 2002 Dec;27(6):421-9.
743 3. Kaushik S, Cuervo AM. The coming of age of chaperone-mediated autophagy. Nat
744 Rev Mol Cell Biol. 2018 Jun;19(6):365-381.
745 4. Chiang HL, Terlecky SR, Plant CP, et al. A role for a 70-kilodalton heat shock protein
746 in lysosomal degradation of intracellular proteins. Science. 1989 Oct 20;246(4928):382-5.
747 5. Cuervo AM, Dice JF. A receptor for the selective uptake and degradation of proteins
748 by lysosomes. Science. 1996 Jul 26;273(5274):501-3.
749 6. Sveger T. The natural history of liver disease in alpha 1-antitrypsin deficient
750 children. Acta Paediatr Scand. 1988 Nov;77(6):847-51.
751 7. Stoller JK, Aboussouan LS. A review of alpha1-antitrypsin deficiency. Am J Respir
752 Crit Care Med. 2012 Feb 1;185(3):246-59.
753 8. Wood AM, Stockley RA. Alpha one antitrypsin deficiency: from gene to treatment
754 [Review]. Respiration; international review of thoracic diseases. 2007;74(5):481-92.
755 9. Stockley RA, Miravitlles M, Vogelmeier C, et al. Augmentation therapy for alpha-1
756 antitrypsin deficiency: towards a personalised approach. Orphanet journal of rare diseases.
757 2013;8:149.
758 10. Qu D, Teckman JH, Omura S, et al. Degradation of a mutant secretory protein,
759 alpha1-antitrypsin Z, in the endoplasmic reticulum requires proteasome activity. J Biol Chem.
760 1996 Sep 13;271(37):22791-5.
761 11. Kamimoto T, Shoji S, Hidvegi T, et al. Intracellular inclusions containing mutant
762 alpha1-antitrypsin Z are propagated in the absence of autophagic activity. J Biol Chem. 2006
763 Feb 17;281(7):4467-76.
764 12. Leon C, Bouchecareilh M. The Autophagy Pathway: A Critical Route in the Disposal
765 of Alpha 1-Antitrypsin Aggregates That Holds Many Mysteries. Int J Mol Sci. 2021 Feb 13;22(4).
766 13. Orenstein SJ, Cuervo AM. Chaperone-mediated autophagy: molecular mechanisms
767 and physiological relevance. Semin Cell Dev Biol. 2010 Sep;21(7):719-26.
768 14. Wu T, Hu E, Xu S, et al. clusterProfiler 4.0: A universal enrichment tool for
769 interpreting omics data. Innovation (Camb). 2021 Aug 28;2(3):100141.
770 15. Crowley LC, Christensen ME, Waterhouse NJ. Measuring Mitochondrial
771 Transmembrane Potential by TMRE Staining. Cold Spring Harb Protoc. 2016 Dec 1;2016(12).
772 16. Crouch SP, Kozlowski R, Slater KJ, et al. The use of ATP bioluminescence as a
773 measure of cell proliferation and cytotoxicity. J Immunol Methods. 1993 Mar 15;160(1):81-8.
774 17. Mulgrew AT, Taggart CC, McElvaney NG. Alpha-1-antitrypsin deficiency: current
775 concepts. Lung. 2007 Jul-Aug;185(4):191-201.
776 18. Mindell JA. Lysosomal acidification mechanisms. Annu Rev Physiol. 2012;74:69-86.
777 19. Zhang J, Johnson JL, He J, et al. Cystinosin, the small GTPase Rab11, and the Rab7
778 effector RILP regulate intracellular trafficking of the chaperone-mediated autophagy receptor
779 LAMP2A. J Biol Chem. 2017 Jun 23;292(25):10328-10346.
780 20. Cuervo AM, Dice JF. Unique properties of lamp2a compared to other lamp2

781 isoforms. Journal of Cell Science. 2000;113(24):4441-4450.
782 21. Cuervo AM, Knecht E, Terlecky SR, et al. Activation of a selective pathway of
783 lysosomal proteolysis in rat liver by prolonged starvation. Am J Physiol. 1995 Nov;269(5 Pt
784 1):C1200-8.
785 22. Massey AC, Kaushik S, Sovak G, et al. Consequences of the selective blockage of
786 chaperone-mediated autophagy. Proc Natl Acad Sci U S A. 2006 Apr 11;103(15):5805-10.
787 23. Gamerdinger M, Kaya AM, Wolfrum U, et al. BAG3 mediates chaperone-based
788 aggresome-targeting and selective autophagy of misfolded proteins. EMBO Rep. 2011
789 Feb;12(2):149-56.
790 24. Kaushik S, Massey AC, Mizushima N, et al. Constitutive activation of chaperone-
791 mediated autophagy in cells with impaired macroautophagy. Mol Biol Cell. 2008
792 May;19(5):2179-92.
793 25. Fujita N, Itoh T, Omori H, et al. The Atg16L complex specifies the site of LC3
794 lipidation for membrane biogenesis in autophagy. Mol Biol Cell. 2008 May;19(5):2092-100.
795 26. Xu Y, Zhang Y, García-Cañaveras JC, et al. Chaperone-mediated autophagy regulates
796 the pluripotency of embryonic stem cells. Science. 2020 Jul 24;369(6502):397-403.
797 27. Anguiano J, Garner TP, Mahalingam M, et al. Chemical modulation of chaperone-
798 mediated autophagy by retinoic acid derivatives. Nat Chem Biol. 2013 Jun;9(6):374-82.
799 28. Saitoh T, Fujita N, Jang MH, et al. Loss of the autophagy protein Atg16L1 enhances
800 endotoxin-induced IL-1beta production. Nature. 2008 Nov 13;456(7219):264-8.
801 29. Ishibashi K, Uemura T, Waguri S, et al. Atg16L1, an essential factor for canonical
802 autophagy, participates in hormone secretion from PC12 cells independently of autophagic
803 activity. Mol Biol Cell. 2012 Aug;23(16):3193-202.
804 30. Liang XH, Jackson S, Seaman M, et al. Induction of autophagy and inhibition of
805 tumorigenesis by beclin 1. Nature. 1999 Dec 9;402(6762):672-6.
806 31. Kang R, Zeh HJ, Lotze MT, et al. The Beclin 1 network regulates autophagy and
807 apoptosis. Cell Death & Differentiation. 2011 2011/04/01;18(4):571-580.
808 32. Pérez-Luz S, Lalchandani J, Matamala N, et al. Quantitative Lipid Profiling Reveals
809 Major Differences between Liver Organoids with Normal Pi*M and Deficient Pi*Z Variants of
810 Alpha-1-antitrypsin. Int J Mol Sci. 2023 Aug 5;24(15).
811 33. Zorova LD, Popkov VA, Plotnikov EY, et al. Mitochondrial membrane potential. Anal
812 Biochem. 2018 Jul 1;552:50-59.
813 34. Dikic I. Proteasomal and Autophagic Degradation Systems. Annu Rev Biochem.
814 2017 Jun 20;86:193-224.
815 35. Hidvegi T, Ewing M, Hale P, et al. An autophagy-enhancing drug promotes
816 degradation of mutant alpha1-antitrypsin Z and reduces hepatic fibrosis. Science. 2010 Jul
817 9;329(5988):229-32.
818 36. Fregno I, Fasana E, Bergmann TJ, et al. ER-to-lysosome-associated degradation of
819 proteasome-resistant ATZ polymers occurs via receptor-mediated vesicular transport. EMBO J.
820 2018 Sep 3;37(17).
821 37. Kaushik S, Cuervo AM. Chaperone-mediated autophagy: a unique way to enter the
822 lysosome world. Trends in Cell Biology. 2012 2012/08/01/;22(8):407-417.
823 38. Ikami Y, Terasawa K, Sakamoto K, et al. The two-domain architecture of LAMP2A
824 regulates its interaction with Hsc70. Exp Cell Res. 2022 Feb 1;411(1):112986.

825 39. Qiao L, Hu J, Qiu X, et al. LAMP2A, LAMP2B and LAMP2C: similar structures,
826 divergent roles. Autophagy. 2023 Jul 21:1-16.
827 40. Dice JF. Peptide sequences that target cytosolic proteins for lysosomal proteolysis.
828 Trends Biochem Sci. 1990 Aug;15(8):305-9.
829 41. Kaushik S, Cuervo AM. Chaperone-mediated autophagy: a unique way to enter the
830 lysosome world. Trends Cell Biol. 2012 Aug;22(8):407-17.
831 42. Sahu R, Kaushik S, Clement CC, et al. Microautophagy of cytosolic proteins by late
832 endosomes. Dev Cell. 2011 Jan 18;20(1):131-9.
833 43. Teckman JH, An JK, Blomenkamp K, et al. Mitochondrial autophagy and injury in
834 the liver in alpha 1-antitrypsin deficiency. Am J Physiol Gastrointest Liver Physiol. 2004
835 May;286(5):G851-62.
836 44. Ordóñez A, Snapp EL, Tan L, et al. Endoplasmic reticulum polymers impair luminal
837 protein mobility and sensitize to cellular stress in alpha1-antitrypsin deficiency. Hepatology.
838 2013 May;57(5):2049-60.
839 45. Lang BJ, Guerrero ME, Prince TL, et al. The functions and regulation of heat shock
840 proteins; key orchestrators of proteostasis and the heat shock response. Archives of Toxicology.
841 2021 2021/06/01;95(6):1943-1970.
842 46. Ghenea S, Chiritoiu M, Tacutu R, et al. Targeting EDEM protects against ER stress
843 and improves development and survival in C. elegans. PLoS Genet. 2022 Feb;18(2):e1010069.
844 47. Qi M, Zhang J, Zeng W, et al. DNAJB1 stabilizes MDM2 and contributes to cancer
845 cell proliferation in a p53-dependent manner. Biochimica et Biophysica Acta (BBA) - Gene
846 Regulatory Mechanisms. 2014 2014/01/01/;1839(1):62-69.
847 48. Kojic S, Nestorovic A, Rakicevic L, et al. A novel role for cardiac ankyrin repeat
848 protein Ankrd1/CARP as a co-activator of the p53 tumor suppressor protein. Archives of
849 Biochemistry and Biophysics. 2010 2010/10/01/;502(1):60-67.
850 49. Guo S, Booten SL, Aghajan M, et al. Antisense oligonucleotide treatment
851 ameliorates alpha-1 antitrypsin-related liver disease in mice. J Clin Invest. 2014 Jan;124(1):251-
852 61.
853 50. Wooddell CI, Blomenkamp K, Peterson RM, et al. Development of an RNAi
854 therapeutic for alpha-1-antitrypsin liver disease. JCI Insight. 2020 Jun 18;5(12).
855 51. Rao L, Xu Y, Reineke LC, et al. Post-Transcriptional Regulation of Alpha One
856 Antitrypsin by a Proteasome Inhibitor. Int J Mol Sci. 2020 Jun 17;21(12).
857 52. Burrows JA, Willis LK, Perlmutter DH. Chemical chaperones mediate increased
858 secretion of mutant alpha 1-antitrypsin (alpha 1-AT) Z: A potential pharmacological strategy for
859 prevention of liver injury and emphysema in alpha 1-AT deficiency. Proceedings of the National
860 Academy of Sciences of the United States of America. 2000 Feb 15;97(4):1796-801.
861 53. Bouchecareilh M, Hutt DM, Szajner P, et al. Histone deacetylase inhibitor (HDACi)
862 suberoylanilide hydroxamic acid (SAHA)-mediated correction of alpha1-antitrypsin deficiency.
863 J Biol Chem. 2012 Nov 2;287(45):38265-78.
864 54. Mallya M, Phillips RL, Saldanha SA, et al. Small molecules block the polymerization
865 of Z alpha1-antitrypsin and increase the clearance of intracellular aggregates. J Med Chem.
866 2007 Nov 1;50(22):5357-63.
867 55. Lomas DA, Irving JA, Arico-Muendel C, et al. Development of a small molecule that
868 corrects misfolding and increases secretion of Z alpha1 -antitrypsin. EMBO Mol Med. 2021 Mar

5;13(3):e13167.

56. Zhang L, Yu J, Pan H, et al. Small molecule regulators of autophagy identified by an image-based high-throughput screen. Proc Natl Acad Sci U S A. 2007 Nov 27;104(48):19023-8.

57. Finn PF, Mesires NT, Vine M, et al. Effects of small molecules on chaperone-mediated autophagy. Autophagy. 2005 Oct-Dec;1(3):141-5.

58. Bourdenx M, Martín-Segura A, Scrivo A, et al. Chaperone-mediated autophagy prevents collapse of the neuronal metastable proteome. Cell. 2021 May 13;184(10):2696-2714.e25.